Two-Dimensional Droplet Spreading over Random Topographical Substrates

Nikos Savva,[1] Serafim Kalliadasis,[1] and Grigorios A. Pavliotis[2]
[1]Department of Chemical Engineering, Imperial College London, London SW7 2AZ, United Kingdom
[2]Department of Mathematics, Imperial College London, London SW7 2AZ, United Kingdom
(Received 17 August 2009; published 23 February 2010)

We examine theoretically the effects of random topographical substrates on the motion of two-dimensional droplets via statistical approaches, by representing substrate families as stationary random functions. The droplet shift variance at both early times and in the long-time limit is deduced and the droplet footprint is found to be a normal random variable at all times. It is shown that substrate roughness inhibits wetting, illustrating also the tendency of the droplet to slide without spreading as equilibrium is approached. Our theoretical predictions are verified by numerical experiments.

DOI: 10.1103/PhysRevLett.104.084501 PACS numbers: 47.55.D−, 05.10.Gg, 47.15.gm, 68.08.Bc

Front propagation in heterogeneous media occurs in a wide variety of areas in physics, ranging from transport phenomena in porous media and reaction-diffusion-advection systems to crack propagation due to lattice defects [1]. Heterogeneities are always present in natural environments, but quite often the process that generates them is random. In such cases they can be modeled as random noise signals, a more physical and practical assumption than, e.g., periodic ones. An example of front propagation central to interfacial hydrodynamics is that of a moving contact line during liquid spreading on a solid substrate, where heterogeneities usually originate from substrate defects, either chemical [2] or topographical [3].

It is a fundamental problem to understand how random heterogeneities influence the spreading dynamics and the characteristics of contact line propagation. Experimental studies on droplet spreading—a simple prototype for the study of contact line motion—suggest that substrates having highly irregular microscale features, commonly called rough, can influence the dynamics significantly [4]. Wenzel [5] deduced an effective contact angle for a contact line on a rough substrate. Several theoretical studies on equilibrium configurations and deterministic substrates followed [6]. Introducing randomness in the substrate is clearly a realistic way to represent roughness, but the few studies in this direction relied on phenomenological modeling ideas and/or postulated equations [7]. Hence, to date a systematic fluid dynamics treatment based on rational statistical approaches is still lacking. As a result, contact line motion on heterogeneous substrates is far from being well understood, unlike other problems in continuum mechanics, such as porous media.

In this Letter we report the first detailed and systematic study of the qualitative effects of random, small-scale spatial heterogeneities on droplet motion, through the development of appropriate statistical methodologies. The starting point is the recent work in [8] on the motion of two-dimensional (2D), partially wetting droplets over deterministic substrates. The restriction to 2D simplifies the problem and is the first step towards understanding the influence of spatial heterogeneities. The model for the droplet motion gives the evolution of the droplet thickness $H(x, t)$ over a substrate $\eta(x)$. It was derived from the hydrodynamic equations in the Stokes regime, by invoking a long-wave expansion for $H_x \sim \bar{H}/L \sim \alpha_s \ll 1$, where $\bar{H}$ and L are the maximum height and droplet radius, respectively, and α_s is the equilibrium angle prescribed by Young's law, and $\eta_x \sim \bar{\eta}/l \ll 1$, where $\bar{\eta}$ and l are the characteristic amplitude and length scale of the topography, respectively. Restricting our attention on the distinguished limit $\bar{H}/L \sim \bar{\eta}/l$ yields a single equation which in dimensionless form reads:

$$\partial_t H + \partial_x[H^2(H + \lambda)\partial_x^3(H + \eta)] = 0, \tag{1}$$

where $\lambda \ll 1$ is the nondimensional slip length imposed to alleviate the stress singularity that occurs at the moving contact line [9]. Equation (1) describes spreading driven by capillarity and resisted by viscosity: the term $\partial_t H$ results from the viscous fluid motion, and the term $\partial_x[\cdot]$ represents the effect of surface tension and also accounts for the substrate curvature contributing an additional capillary pressure, $-\partial_x^2\eta$. The spatial coordinate x and time t are made nondimensional by $L = \sqrt{A/(2\alpha_s)}$ and $3\mu L/(\gamma\alpha_s^3)$, respectively, where A is the droplet cross-sectional area, μ is the viscosity, and γ is the surface tension. Both $\eta(x)$ and $H(x)$ are scaled by $L\alpha_s$ and λ by $L\alpha_s/3$. Equation (1) is solved subject to (i) a constant area constraint, (ii) the boundary conditions at the contact points, i.e., the droplet thickness vanishes and the angle the free surface makes with the substrate remains equal to its static value α_s. For quasistatic spreading, a singular perturbation method was employed in [8] to asymptotically match the solution in the bulk of the fluid with the solution in the vicinity of the contact lines, leading to a set of two integro-differential equations (IDEs) for the evolution of the right and left contact points at $x = a_{\pm}(t)$, respectively.

Here we use the set of IDEs to investigate the case where $\eta(x)$ is a random function. We take $|\eta(x)| \ll 1$ assuming also that its variations occur at length scales that are much longer than λ. The requirement of substrate smoothness

together with the fact that the "noise" is spatial and enters the equations in a nonlinear fashion precludes casting the problem into the standard Langevin formalism.

The primary fundamental difficulty with the substrate is utilizing a random representation that can have a large frequency content and at the same time is differentiable. A convenient representation is the random function,

$$\eta(x) = \frac{\eta_0}{\sqrt{N}} \sum_{m=1}^{N} \left(\alpha_m \sin\frac{k_0 m}{N} x + \beta_m \cos\frac{k_0 m}{N} x \right), \qquad (2)$$

where η_0 and k_0 are the characteristic amplitude and wave number, respectively, such that $\eta_0 k_0 \ll 1$, and N is a large positive integer. Here α_m and β_m are statistically independent normal variables of unit variance. It is readily seen that $\eta(x)$ is a periodic function with period $2\pi N/k_0$, but we eventually take $N \to \infty$ so that this periodicity is lost and $\eta(x)$ approaches a band-limited white noise [see Fig. 1(a); in this limit, continuity of (2) and all its derivatives can be shown by Kolmogorov's continuity theorem].

An attractive feature of the stochastic representation in (2) is that it generates families of substrate realizations parametrized by two parameters, η_0 and k_0, which are often reported in experimental studies when characterizing a rough substrate. Comparison with experimental substrate profiles determined by Hitchcock *et al.* [3] shows that (2) can be used to realistically represent actual rough substrates. For example, given the experimental profile in Fig. 1(b) (solid line of the upper plots), k_0 is readily determined from $k_0 = 2\pi n/\sqrt{5/3}$ and η_0 from $\eta_0 = \sqrt{\langle \eta^2 \rangle}$, where n corresponds to the number of maxima per unit length [10] and $\langle \cdot \rangle$ denotes an ensemble average over all substrate realizations. To obtain the dashed profile as an approximation to the experimental profile using (2), the finite length of the profile is matched to the period of (2) to get $N = 26$, which then allows us to determine α_m and β_m by projecting the experimental profile onto their corresponding harmonics. On the other hand, the lower plot in Fig. 1(b) is generated with random α_m and β_m with $N = 1000$, where η_0 and k_0 are kept the same so that the lower plot belongs to the same substrate family with the upper one. In the following, a large number of substrate realizations, typically 20 000 with $N = 1000$, will be utilized.

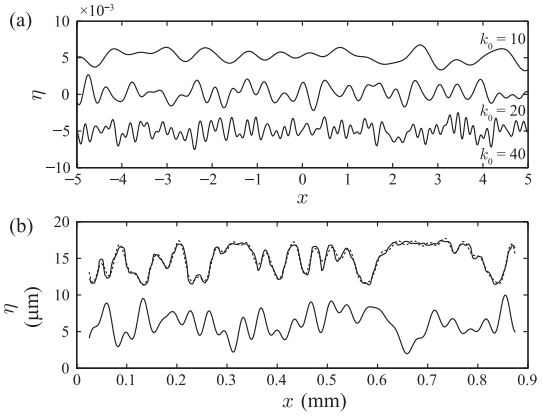

FIG. 1. (a) Sample substrate realizations using (2) for $\eta_0 = 10^{-3}$ and $k_0 = 10$, 20, and 40. (b) Top plot: Solid line: Experimental profile from Hitchcock *et al.* [3] for an alumina sample. Dashed line: Approximation obtained by projecting the experimental profile onto $N = 26$ harmonics in (2). Lower plot: Sample substrate realization for the same η_0 and k_0, but $N = 1000$.

To facilitate the analysis, we introduce the *contact line fluctuation* ε and *droplet shift* ℓ along the substrate (see Fig. 2), defined in terms of the contact line locations as

$$\varepsilon = \frac{1}{2}(a_+ - a_-) - x_0 \quad \text{and} \quad \ell = \frac{1}{2}(a_+ + a_-), \qquad (3)$$

where x_0 is the droplet radius when spreading occurs on a flat substrate, which approaches $\sqrt{3}$ in the long-time limit. Here ℓ is a measure of the distance the droplet midpoint is displaced from $x = 0$, whereas ε measures the deviation of the droplet radius from x_0. Assuming $\eta_0 \ll 1$, we also expect that $\varepsilon \ll 1$, so that linearizing the equations that give the static locations of the contact lines about the flat-substrate equilibrium yields

$$\varepsilon = \frac{3\eta_0}{2\sqrt{N}} \sum_{m=1}^{N} (\alpha_m \sin\lambda_m \ell + \beta_m \cos\lambda_m \ell) I(\sqrt{3}\lambda_m), \qquad (4)$$

$$\sum_{m=1}^{N} (\alpha_m \cos\lambda_m \ell - \beta_m \sin\lambda_m \ell) \mathcal{J}(\sqrt{3}\lambda_m) = 0, \qquad (5)$$

where $\lambda_m = k_0 m/N$, $I(x) = \mathrm{sinc}x - \cos x - (x/3)\sin x$ with $\mathrm{sinc}x = x^{-1}\sin x$ and $\mathcal{J}(x) = x\cos x - \sin x$. The neglected terms of this linearization procedure are small provided that $\eta_0 k_0^2 \ll 1$. To conform with this condition we focus on substrate families with $1 \ll k_0 \ll \eta_0^{-1/2}$. Hence, for a droplet with $L = 0.5$ mm, $\alpha_s = 15°$, and substrate topographies with amplitudes 0.5 μm ($\eta_0 \approx 4 \times 10^{-4}$), $\eta_0 k_0^2 < 1$ for $l > 77$ μm. At such scales, slip is more important than intermolecular forces in controlling the spreading dynamics, as demonstrated in [11]. By the central limit theorem, we also see from (4) that ε is well-approximated as a normally distributed random variable.

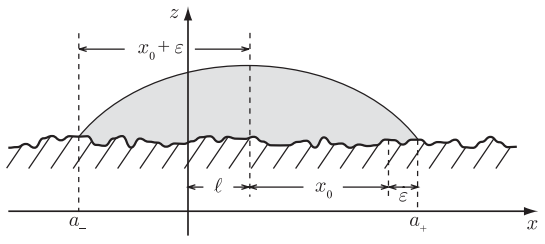

FIG. 2. Droplet lying between $a_- \le x \le a_+$ on a random topographical substrate. The droplet shift, $\ell = \frac{1}{2}(a_+ + a_-)$, is the distance the droplet midpoint moves away from $x = 0$, and the contact line fluctuation, $\varepsilon = \frac{1}{2}(a_+ - a_-) - x_0$, measures deviations of the contact line location away from the flat-substrate radius, $x_0(t)$.

Contributions to its mean are of $\mathcal{O}(\eta_0)$ and originate from $\langle \alpha_m \sin\lambda_m \ell + \beta_m \cos\lambda_m \ell \rangle$. If all equilibria are taken into account however, this quantity vanishes and contributions to the mean are of $\mathcal{O}(\eta_0^2)$. Therefore, to fully assess the effects of spatial heterogeneities, the equilibria attained from the droplet dynamics need to be considered instead.

The IDEs obtained for deterministic substrates in [8] are appropriately modified to model random spatial heterogeneities described by (2) and are linearized for $\varepsilon \ll 1$. This calculation is rather involved and lengthy. The final equations are of the form

$$\dot{\varepsilon} + \mathcal{A}(t)\varepsilon = \frac{\eta_0}{\sqrt{N}} \sum_{m=1}^{N} (\alpha_m \sin k_m \ell + \beta_m \cos k_m \ell)\mathcal{B}(t, k_m),$$

$$\dot{\ell} = \frac{\eta_0}{\sqrt{N}} \sum_{m=1}^{N} (\alpha_m \cos k_m \ell - \beta_m \sin k_m \ell)\mathcal{C}(t, k_m),$$

where $\mathcal{A}(t)$, $\mathcal{B}(t, k_m)$, and $\mathcal{C}(t, k_m)$ are complicated functions of their arguments. Their time dependence enters through x_0 and its time derivative with x_0 satisfying $3\dot{x}_0 \ln[2x_0/(\lambda e^2)] = 27x_0^{-6} - 1$. The linearity of the equation for ε implies that it is a normal variable for all times, whose variance may be computed explicitly. Figure 3(a) shows plots of the standard deviation of ε, σ_ε, as a function of time for $\eta_0 = 5 \times 10^{-4}$ and $k_0 = 20$, 30, and 40. When $k_0 = 20$, the theoretically predicted curve is indistinguishable from the one obtained from numerical experiments, but the agreement tends to degrade as the condition $\eta_0 k_0^2 \ll 1$ no longer holds. Determining the time evolution of the standard deviation of ℓ, σ_ℓ, explicitly is a formidable task due to the highly nonlinear nature of the equation for ℓ, but the early-time behavior can be found by linearizing about $\ell = 0$. In Fig. 3(b) we show the evolution of σ_ℓ as computed from numerical experiments, together with the early-time behavior predicted by the linear theory for the same parameters as in Fig. 5(b). There is excellent agreement up to $t \sim \mathcal{O}(30)$. Comparing the time scales over which σ_ε and σ_ℓ saturate reveals that the droplet "footprint," $2(\varepsilon + x_0)$, approaches equilibrium over a shorter time scale compared to the time for ℓ to reach equilibrium, which suggests that the droplet slides without spreading along the various substrate features to find the final equilibrium position. In the long-time limit, we cannot solve for ℓ explicitly since (5) is nonlinear and also admits infinitely many solutions. However, the evolution towards equilibrium fixes the solution to (5) to be the stable equilibrium that is closest to $\ell = 0$, a problem which is reminiscent of the highly nontrivial "first-passage problem" in probability theory [10]. Interestingly, Fig. 4(a) reveals that the probability density of ℓ as $t \to \infty$, p_ℓ, is far from being a normally distributed random variable. By taking into account the mean distance between zeros of (5) [10], together with the fact that on average half of the closest equilibria are unstable, we find that

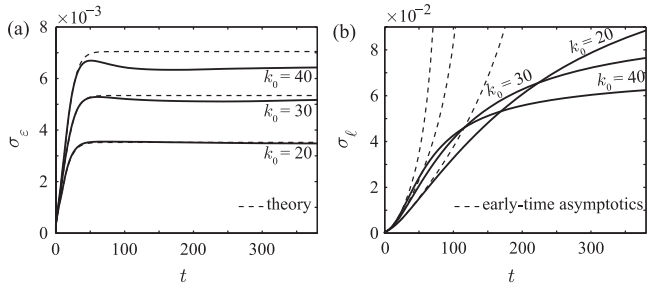

FIG. 3. Spreading dynamics for $\eta_0 = 5 \times 10^{-4}$ and $k_0 = 20$, 30, and 40. (a) Standard deviation of ε as a function of time. The numerical experiments (solid line) are indistinguishable from theory (dashed line) for $k_0 = 20$. (b) Standard deviation of ℓ as a function of time. The early-time asymptotics agree with numerical experiments up to $t \sim \mathcal{O}(30)$. For large times the solid lines asymptote at values predicted from the long-time analysis.

$$\sigma_\ell^2 = \frac{5}{6}\pi^2 k_0^{-2}\left(1 - \frac{1}{2}\mathrm{sinc}2\sqrt{3}k_0\right) + \mathcal{O}(k_0^{-4}) \qquad (6)$$

for $k_0 \gg 1$. Clearly, as the substrate features become rougher the droplet has a tendency to shift or slide less along the substrate. This behavior is confirmed in Fig. 4(b), where we plot the theoretically predicted σ_ℓ as a function of k_0 together with numerical experiments for different substrate families, confirming also the independence of ℓ on η_0.

From our numerical experiments we also found that $\langle \varepsilon \rangle < 0$ in the long-time limit, thus suggesting that surface roughness inhibits wetting. Such behavior appears to contradict Wenzel's theory, but it signifies the fact that the droplet has to overcome the energy barriers that separate the multiple equilibrium droplet states. This effect is demonstrated in the recent experiments of Chung *et al.* [12], where spreading perpendicular to the grooves of parallel-grooved substrates violates Wenzel's law, and is further supported by the work of Cox [6] on wedge equilibria over (deterministic) three-dimensional rough substrates, who postulated that roughness-induced wetting enhancement is due to a higher-order effect which manifests itself when spreading does not occur perpendicular to the substrate grooves. A semianalytical expression for $\langle \varepsilon \rangle$ can be obtained by noting that, from our numerical experiments, $\langle \alpha_m \sin\lambda_m \ell + \beta_m \cos\lambda_m \ell \rangle = F(k_0)\mathcal{J}(\sqrt{3}\lambda_m)/(k_0\sqrt{3})$, where F appears to depend weakly on η_0 and k_0 and equals 3 for $\eta_0 k_0^2 \ll 1$. Based on this, $\langle \varepsilon \rangle$ is found to be

$$\langle \varepsilon \rangle_{\mathrm{approx}} \approx -\frac{3}{8}\eta_0(2 - \cos 2\sqrt{3}k_0) + \mathcal{O}(\eta_0 k_0^{-1}), \qquad (7)$$

for $k_0 \gg 1$. This implies that the mean apparent contact angle increases by an amount $2|\langle \varepsilon \rangle|/\sqrt{3}$ to leading order in ε. Figure 5(a) depicts a plot of (7) as a function of k_0 together with the mean obtained in numerical simulations for substrates with $\eta_0 = 10^{-3}$. For smaller k_0, the agreement between the semianalytic approximation and the numerical experiments is evident, but as the substrate becomes more rough so that $\eta_0 k_0^2 \ll 1$ is violated and nonlinear effects become appreciable, there is a clear deviation towards a progressive reduction of the mean

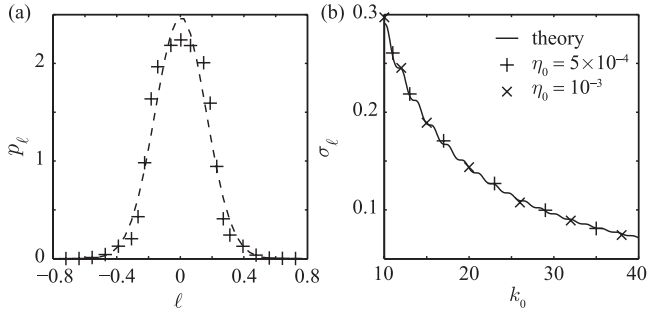

FIG. 4. Statistics of ℓ for k_0 ranging from 10 to 40 with $\eta_0 = 5 \times 10^{-4}$ (+) and 10^{-3} (×). (a) Probability density function of ℓ when $\eta_0 = 5 \times 10^{-4}$ and $k_0 = 20$ compared with a normal density of the same variance (dashed line). (b) Standard deviation of ℓ as a function of k_0, illustrating the excellent agreement of (6) with numerics.

droplet radius. Hence the apparent contact angle tends to increase with substrate roughness, thus pointing towards a substrate-induced, hysteresislike effect.

The variance of ε can be deduced from (4) by converting the Riemann sum into an integral by taking $N \to \infty$,

$$\sigma_\varepsilon^2 = \frac{1}{8}\eta_0^2 k_0^2 (1 - 3\mathrm{sinc}2\sqrt{3}k_0) + \mathcal{O}(\eta_0^2), \qquad (8)$$

when $k_0 \gg 1$. The theoretically predicted σ_ε is in very good agreement with the simulated one as shown in Fig. 5(b), where we plot σ_ε as a function of k_0 when $\eta_0 = 5 \times 10^{-4}$ and $\eta_0 = 10^{-3}$. Different substrate descriptions might have been used, as, for example, representations that exhibit statistical self-affinity, whose spectral density follows the power law $\propto k^{2D-5}$ [13], where $1 < D < 2$ is the fractal dimension. The differentiability requirement of $\eta(x)$ together with the fact that in reality a self-affine structure cannot persist for all length scales requires imposing lower and upper wave number cutoffs. However, the results are qualitatively the same since the leading-order

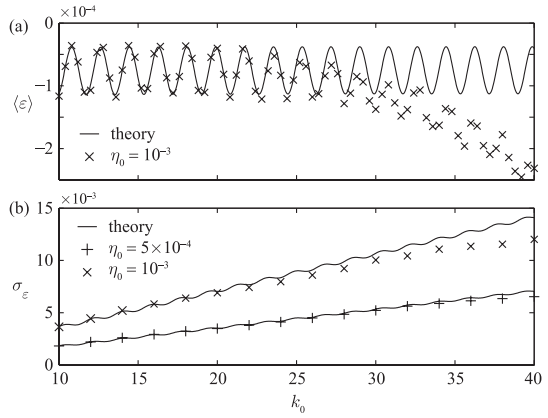

FIG. 5. Statistics of ε for the same parameters as in Fig. 4. (a) Comparison of the numerically determined $\langle\varepsilon\rangle$ and $\langle\varepsilon\rangle_{\text{approx}}$ as a function of k_0. (b) Comparison of the theoretical and numerical σ_ε as a function of k_0. The agreement is excellent for $\eta_0 k_0^2 \ll 1$.

variance of ε differs from the leading order of (8) only by a factor $3(2 - D)(g^{4-2D} - g^2)/[(D - 1)(1 - g^{4-2D})]$, that depends on two additional parameters, namely, D and the lower to upper cutoff wave number ratio g. Numerical studies of σ_ℓ also confirm qualitative agreement.

To conclude, we have presented the first detailed and systematic investigation of the motion of 2D droplet fronts over randomly varying shallow substrates by using a model derived from first principles. Droplet equilibria alone cannot fully determine the effects of random substrates on wetting. For arbitrary times, the evolution of ℓ and ε suggests that on average the droplet has the tendency to slide without spreading along the substrate before reaching equilibrium. In the long-time limit, ℓ and ε scale with $\sigma_\varepsilon^2 \sim \eta_0^2 k_0^2$ and $\sigma_\ell^2 \sim k_0^{-2}$, respectively. We believe that these results will motivate further analytical and experimental studies on the role of heterogeneities on wetting hydrodynamics.

We thank the anonymous referee for suggesting the statistical self-affine substrate representation. We acknowledge financial support from EPSRC Platform Grant No. EP/E046029.

[1] G. M. Homsy, Annu. Rev. Fluid Mech. **19**, 271 (1987); R. B. Philips, *Crystals, Defects and Microstructures* (Cambridge University Press, Cambridge, England, 2001); J. Xin, SIAM Rev. **42**, 161 (2000).
[2] L. W. Schwartz and R. R. Elley, J. Colloid Interface Sci. **202**, 173 (1998); L. W. Schwartz, Langmuir **14**, 3440 (1998); T. Cubaud and M. Fermigier, J. Colloid Interface Sci. **269**, 171 (2004).
[3] S. J. Hitchcock, N. T. Caroll, and M. G. Nicholas, J. Mater. Sci. **16**, 714 (1981); S. Shibuichi *et al.*, J. Phys. Chem. **100**, 19 512 (1996); J. Bico, C. Tordeaux, and D. Quéré, Europhys. Lett. **55**, 214 (2001).
[4] A. M. Cazabat and M. A. Cohen-Stuart, J. Phys. Chem. **90**, 5845 (1986).
[5] R. N. Wenzel, Ind. Eng. Chem. **28**, 988 (1936).
[6] R. E. Johnson and R. H. Dettre, Adv. Chem. Ser. **43**, 112 (1964); L. M. Hocking, J. Fluid Mech. **76**, 801 (1976); C. Huh and S. G. Mason, J. Colloid Interface Sci. **60**, 11 (1977); R. G. Cox, J. Fluid Mech. **131**, 1 (1983); J. F. Joanny and P.-G. de Gennes, J. Chem. Phys. **81**, 552 (1984).
[7] K. M. Jansons, J. Fluid Mech. **154**, 1 (1985); C. Borgs *et al.*, Phys. Rev. Lett. **74**, 2292 (1995); S. Moulinet, C. Guthmann, and E. Rolley, Eur. Phys. J. E **8**, 437 (2002); A. Tanguy and T. Vettorel, Eur. Phys. J. B **38**, 71 (2004).
[8] N. Savva and S. Kalliadasis, Phys. Fluids **21**, 092102 (2009).
[9] C. Huh and L. E. Scriven, J. Colloid Interface Sci. **35**, 85 (1971).
[10] S. O. Rice, Bell Syst. Tech. J. **23**, 282 (1944); **24**, 46 (1945).
[11] L. M. Hocking, Phys. Fluids **6**, 3224 (1994).
[12] J. Y. Chung, J. P. Youngblood, and C. M. Stafford, Soft Matter **3**, 1163 (2007).
[13] A. Majumdar and C. L. Tien, Wear **136**, 313 (1990).